ChemMedChem

Chemistry Europe
European Chemical Societies Publishing

Accepted Article

Title: Acyl Derivatives of Eudesmanolides to Boost their Bioactivity. An Explanation of Behavior in the Cell Membrane Using a Molecular Dynamics Approach.

Authors: Francisco J.R. Mejías, Alexandra G. Durán, Jesús G. Zorrilla, Rosa M. Varela, José M.G. Molinillo, Manuel M. Valdivia, and Francisco A. Macias

To be cited as: *ChemMedChem* 10.1002/cmdc.202000783

Link to VoR: https://doi.org/10.1002/cmdc.202000783

WILEY-VCH

WILEY-VCH

FULL PAPER

Acyl Derivatives of Eudesmanolides to Boost their Bioactivity. An Explanation of Behavior in the Cell Membrane Using a Molecular Dynamics Approach.

Francisco J.R. Mejías[a], Dr. Alexandra G. Durán[a], Jesús G. Zorrilla[a], Prof. Rosa M. Varela[a], Prof. José M.G. Molinillo[a], Prof. Manuel M. Valdivia[b], Prof. Francisco A. Macías*[a]

[a] F.J.R. Mejías, Dr. A.G. Durán, J.G. Zorrilla, Prof. R.M. Varela, Prof. J.M.G. Molinillo and Prof. F.A. Macías
Allelopathy Group, Department of Organic Chemistry, Institute of Biomolecules (INBIO), Campus de Excelencia Internacional (ceiA3), School of Science, University of Cádiz, C/República Saharaui, 7, 11510, Puerto Real, Cádiz, Spain.
E-mail: famacias@uca.es

[b] Prof. M.M. Valdivia
Department of Biomedicine, Biotechnology and Public Health, Institute of Biomolecules (INBIO), School of Science, University of Cádiz, C/República Saharaui, 7, 11510, Puerto Real, Cádiz, Spain.

Supporting information for this article is given via a link at the end of the document.

Abstract: Semi-synthetic analogs of natural products provide an important approach to obtain safer and more active drugs and they also have enhanced physicochemical properties such as persistence, cross membrane processes and bioactivity. Acyl derivatives of different natural product families, from sesquiterpene lactones to benzoxazinoids, have been synthesized and tested in our laboratories. These compounds were evaluated against tumoral and non-tumoral cell lines to identify selective derivatives with reduced negative impact upon application. The mode of action of these compounds was analyzed by anti-caspase-3 assays and molecular dynamics simulations with cell membrane recreation were also carried out. Aryl derivatives of eudesmanolide stand out from the other compounds and are better than current anti-cancer drugs, such as etoposide, in terms of selectivity and activity. Computational studies provide evidence that lipophilicity plays a key role and the 4-fluorobenzoyl derivative can pass easily through the cell membrane.

Introduction

Natural product research has produced the majority of medicinal drugs that are successfully tested in phase II clinical trials. Nevertheless, just 20% of these natural product leads are taken through unchanged to the final drug product.[1] Thus, small structural modifications to generate derivative banks could produce new and effective drugs with improved bioactivity profiles, as well as better absorption, distribution, metabolism and excretion properties.

In this respect, hydroxylated costunolide (**1**) derivatives can be highlighted as a source of potent drugs with several types of bioactivity. Reynosin (**2**) and santamarine (**3**) (Figure 1) have shown strong bactericidal activity against *Mycobacterium tuberculosis*, with a minimal inhibitory concentration of 64 μg/mL.[2] In addition, reynosin also suppresses ROS production and reduces COX-2 levels via the NF-KB pathway.[3,4] *In vivo* studies have recently been carried out on this eudesmanolide, with hepatoprotective effects observed in mouse liver upon exposure to thioacetamide in order to generate apoptosis.[5] Furthermore, reynosin (**2**) seems to be relevant in neural protection against Parkinson's diseases.[6] Semi-synthetic analogs of this relevant natural product seem to be important to enhance the inhibition of the tumor necrosis factor-alpha, and simple derivatizations – such as hydroxylation – were key to enhancing the activity.[7] In spite of the abundant publications on these natural products, simple ester derivatives obtained from hydroxyl-substituted precursors have not been developed to evaluate their activity by modulation of the physicochemical properties. Furthermore, aromatic derivatives mono-halogenated, and specifically mono-fluorinated seems to be essential in new strategies to stop cancer progression. This is the case of quinazoline 4-fluorophenyl derivatives, which inhibits Hsp90, and also the case of the 4'-fluoro-2'-hydroxy-chalcone derivatives which show anti-inflammatory effects.[8–10] Thus, synthesis of reynosin (**2**) derivatives focusing in halogenated compound could be a relevant starting point.

Natural products with other types of skeletons are also relevant in medicinal chemistry. For example, sesquiterpene lactones with a guaiane-type skeleton, e.g., cynaropicrin (**12**) and its derivatives, have shown anti-proliferation of leukocyte cancer cell lines.[11] In the case of benzoxazinoids, like APO (**14**) and its mimics (**16** and **18**), application against prostate cancer not only showed favorable results in cell lines,[12] but even in human assays where a benzoxazinoid-rich diet was applied.[13] Diterpenes such as gummiferolic acid (**20**) also have broad applications in medicine, specifically to promote proliferation of neural precursor cells when tested in neurosphere assays.[14]

In the work described here, costunolide was isolated from the roots of *Saussurea costus* and reynosin was synthesized to obtain acyl derivatives by reaction with the hydroxyl functional group. A structure-activity relationship study was performed to evaluate the effect of bioavailability of the reynosin derivatives, and the IC_{50} values were obtained for cytotoxicity on HeLa cells. After selection of the best derivative, caspase-3 assays were carried out to analyze the mode of action, and an HEK cell bioassay was carried out to ascertain the selectivity of the compounds against tumoral targets. Simulation by molecular dynamics in the cell membrane allowed the stability and ease of membrane crossing processes to be analyzed. In order to understand the relevance of the best acyl fragment, different esters of other natural products and mimics with different skeletons or families were synthesized to evaluate their bioactivity.

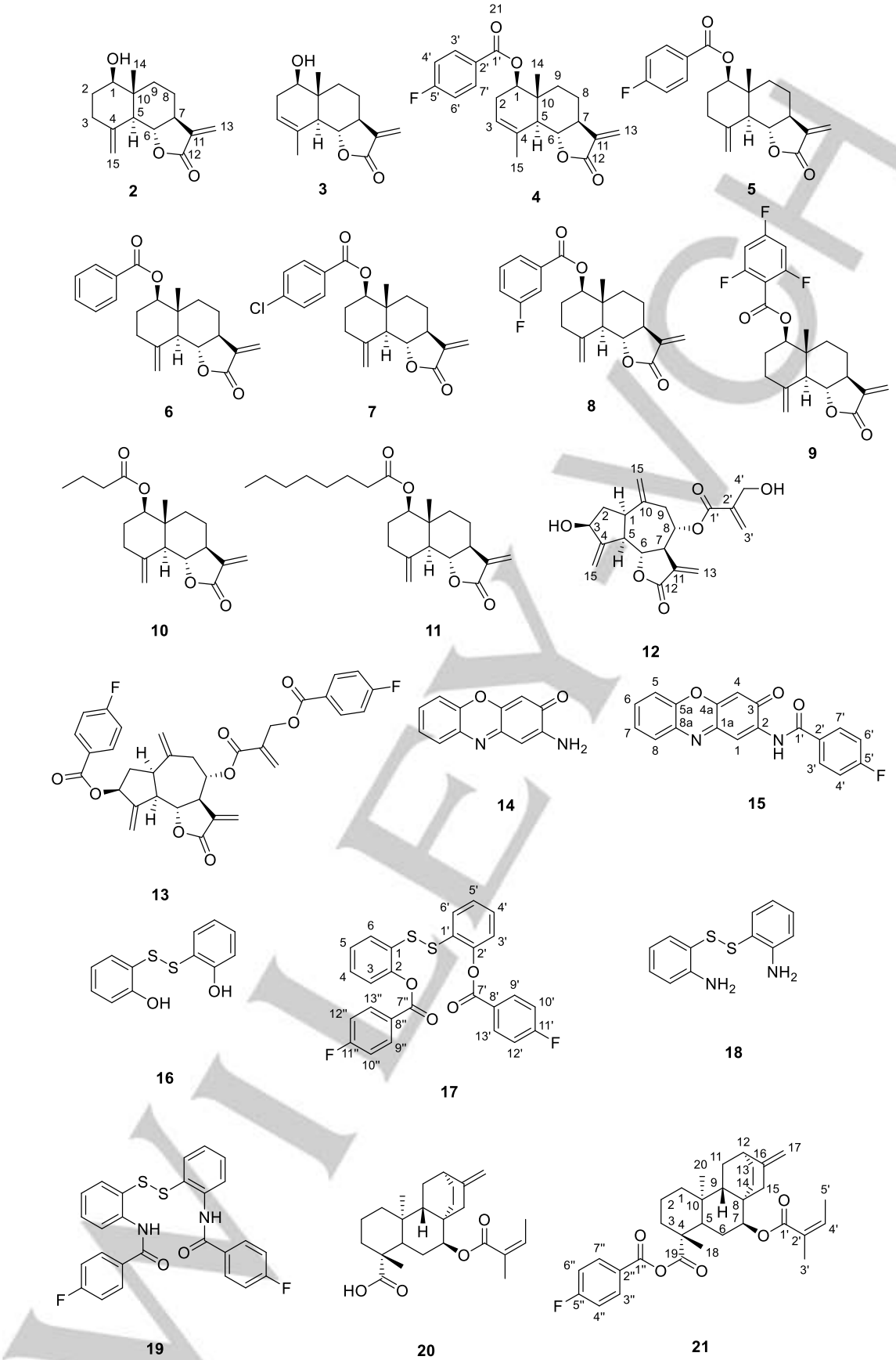

Figure 1. Isolated and synthesized compounds employed in this study.

Results and Discussion

Synthesis of reynosin derivatives

The starting material **1** (Figure 2) was isolated in high yield from roots of *Saussurea costus*, as described in the Experimental Section. This compound was transformed into the target eudesmanolides by a cyclization reaction in the presence of the epoxidation agent *m*-CPBA followed by the addition of a catalytic amount of *p*-TsOH in order to open the epoxy ring. Compounds **2** and **3** were generated in 31% and 51% yield, respectively.
The synthesis of acyl derivatives (Figure 2) was carried out at room temperature in pyridine and this approach gave high yields of compounds **4**–**11**. A molar excess of acyl chloride is usually employed in this kind of reaction to avoid yield loss due to side reactions to give carboxylic acids. Extraction with 1.0 M NaOH was employed to remove acid derivatives formed by hydrolysis of the acyl chlorides. The synthesized aryl derivatives enabled an analysis of the influence of the inclusion of halogen(s), the position of the halogen atom and the number of halogens in the reynosin derivatives. The study carried out on the alkyl derivatives (**10**–**11**) showed the influence that the lipophilicity of reynosin by comparison with the aryl compounds.

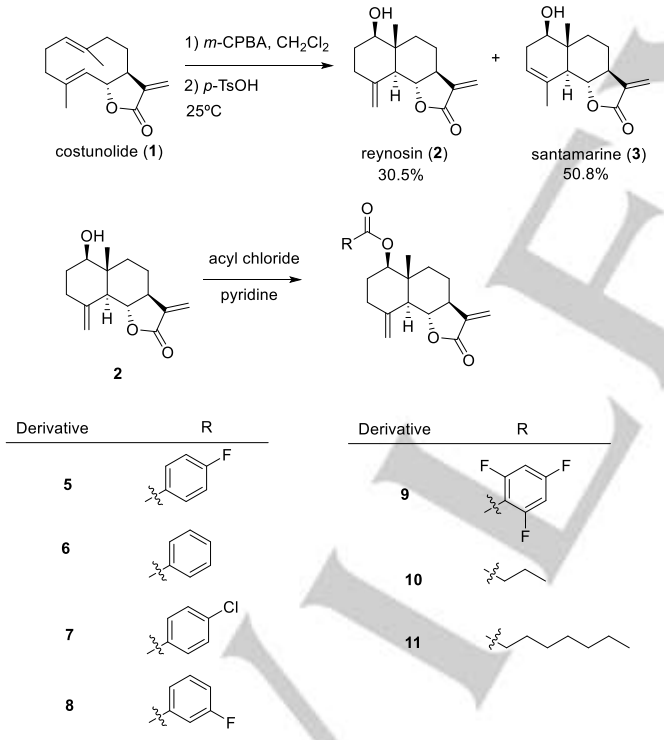

Figure 2. Synthesis of hydroxylated eudesmanolides reynosin and santamarine. Synthesis of ester derivatives of reynosin with aryl fragments and aliphatic fragments.

In the ^{1}H NMR spectra the H-1 signal for the eudesmane skeleton was shifted the most after acylation. The aromatic ring at the three position still had a marked influence and this increased the proton shift from 4.80 (butyryl) or 4.79 ppm (octanoyl) to 5.04–5.07 ppm (aromatic derivatives). In the case of compound **10**, the H-2' and H-3' signals caused a loss of resolution in the signals for H-2 and H-5 due to their large integral, which broadened the baseline and made it difficult to measure some of the coupling constants. Nevertheless, this behavior was more pronounced for compound **11**, for which the H-3' to H-7' signals fully overlapped those of H-2 and H-5.

It is known that fluorine atoms show NMR activity due to the more abundant isotope ^{19}F, which has a nuclear spin of ½. This impacts not only the ^{1}H NMR spectra but ^{13}C NMR spectra and it causes significant multiplicities. When one fluoro-substituent is present on the aromatic ring, the *ortho*-carbon signal appears as a doublet (J = 21–23 Hz) The *meta*-carbon signal is also doublet, but its coupling constant is limited to the range 7.5–10.0 Hz. The carbon in the *para*-position has the smallest coupling constant, with a value in the range 2.8–4.0 Hz. In contrast, the carbon that is bonded to the fluoro-substituent has the largest constant (250.0–255.0 Hz). In the case of multiple fluorine substitution, e.g., the 2,4,6-trifluoro derivative (**9**), the coupling constant exceeds the ranges mentioned above due to high electronegativity of each fluorine nucleus. The carbon directly linked to the fluorine atom has a doublet multiplicity with J >258 Hz and the *ortho*, *meta* and *para* coupling constants showed Δ5 Hz in comparison with the mono-fluorinated derivative.

In the aliphatic derivatives, i.e., butyryl (**10**) and octanoyl (**11**), the ^{13}C spectra were simplified due to the absence of ^{19}F. Nevertheless, the large numbers of protons with similar chemical environments meant that the ^{1}H spectra between 2.00 and 0.50 ppm contained a large number of signals with high integral values. The H-2'a and H-2'b signals were shifted the most due to their proximity to the carbonyl group (α-carbon). In these two cases signals were observed at 2.29 and 2.30 ppm, respectively, with coupling constants in the range 7.2–7.3 Hz. However, the coupling constants for the adjacent protons were in the range 1.7–1.2 ppm. These higher field signals were overlapped for the octanoyl derivative (**11**).

Bioactivity studies

The pharmacological potential of reynosin has been described in previous publications, including anticancer properties.[15,16] One of the main purposes of the present work was to synthesize reynosin analogs in an effort to improve the bioavailability and biological properties. The ultimate aim was to design new and potent drugs. In the first step, seven acyl derivatives were obtained by modifying the hydroxyl group on the reynosin backbone (**5**–**11**). The cytotoxicity vales of these compounds were assessed on cervical carcinoma cells (HeLa) at 100 µM for 24 hours (Figure 3).

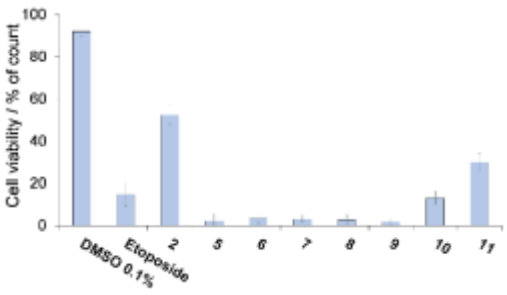

Figure 3. Cell viability by dye exclusion against cervical carcinoma cells (HeLa). 1-*O*-Acyl reynosin derivatives were evaluated at 100 µM after 24 h of treatment. Data are expressed as mean ± SD (n = 3).

It has been demonstrated in several studies that lipophilicity is an important factor for biological effects.[17,18] Thus, it has been noted that the presence, or an increasing number, of hydroxyl groups in the sesquiterpene lactone backbone results in lower antimycobacterial, fungicidal and cytotoxic activities.[19,20] On the other hand, the α-methylene-γ-lactone moiety is considered to be an essential structural requirement for significant cytotoxic activity.[21] As a consequence, all of the derivatives synthesized in this work contain this framework. The results show that modification of the hydroxyl group on the reynosin skeleton leads to a significant improvement in the activity (Figure 3). Derivatives with an aromatic group (**4**–**9**) were more active than those with a linear chain (**10**–**11**). In terms of activity it is worth highlighting compounds **5** and **9**.

In view of the findings outlined above, the 4-fluorobenzoyl framework was selected to modify other mimics and natural compounds. Two additional sesquiterpene lactones (santamarine (**3**) and cynaropicrin (**12**)), 2-amino-3*H*-phenoxazin-3-one (APO (**14**)), two benzoxazinoid mimics (**16** and **18**) and a diterpene (gummiferolic acid (**20**)) were selected for the next study. Moreover, in cases where hydrolysis of the ester bond occurred, the activity observed may be due to 4-fluorobenzoic acid and this compound was also tested.

The results of the cytotoxicity study are shown in Figure 4. The most potent cytotoxic effects were observed when the 4-fluorobenzoyl unit was introduced onto the santamarine skeleton (**4**). In this case a cell viability value below 5% obtained, thus highlighting the relevance of the eudesmane skeleton. Nevertheless, modification of cynaropicrin (**12**) did not lead to an improvement in the anti-proliferative activity against the tumor cells. This finding could be due to the increased lipophilicity (Table 1), with a CLog P value of 5.83, in respect of the established 'Lipinski's rule of five' for pharmaceutical candidates.[22] In the case of benzoxazinoids and their mimics, the introduction of this framework into the APO (**14**) core also caused a loss of cytotoxic activity (derivative **15**). This result indicates that the molecular site of action had been modified and the amino group is essential to retain the biological activity. On the other hand, modification of benzoxazinoid mimic **16** gave the new derivative **17**, which had a four-fold higher anti-proliferative activity. However, this variation was not observed for benzoxazinoid mimic **18**, as the level of activity of its derivative (**19**) increased only slightly. Similar behavior was also observed on modifying the gummiferolic acid (**20**) core to afford derivative **21**. In both of these cases the pharmacophore was not affected. Overall, the modification of amino groups to form amide derivatives led to a decrease in the activity, while ester formation on the hydroxyl groups resulted in an increase in cytotoxic activity. It is also worth highlighting that 4-fluorobenzoic acid did not display any activity. Thus, the activity observed was due solely to the chemical compound tested.

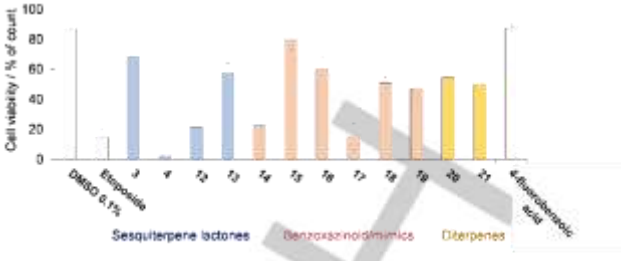

Figure 4. Cell viability by dye exclusion against cervical carcinoma cells (HeLa). 4-Fluorobenzoyl derivatives were evaluated at 100 µM for 24 h. Experiments were performed in triplicate and data are expressed as mean ± SD.

Results observed to every aromatic derivative of reynosin (**2**) are statistically similar, highlighting mono-fluorinated and tri-fluorinated derivatives. According to literature, mono-halogenated derivatives are broadly applied in biological studies and present better results due to lower persistence and better absorption and distribution *in vivo*.[8–10,23]In view of the results outlined above, three promising derivatives (**4**, **5** and **17**) were selected, on the basis of their high activity levels, to perform a cell viability study at various concentrations (from 0.1 to 100 µM) in tumoral (HeLa) and non-tumoral (HEK-293, human embryonic kidney) cell lines for 24 h to study their selectivity. The data were compared to those of the clinically used anticancer drug etoposide (Figure 5).

Table 1. Lipophilicity values for each compound. CLog P values calculated with ChemDraw Professional® v. 17.1.

Compound	CLog P
Reynosin (**2**)	1.183
Santamarine (**3**)	1.183
4-Fluorobenzoylsantamarine (**4**)	4.201
4-Fluorobenzoylreynosin (**5**)	4.201
Benzoylreynosin (**6**)	4.058
4-Chlorobenzoylreynosin (**7**)	4.771
3-Fluorobenzoylreynosin (**8**)	4.201
2,4,6-Trifluorobenzoylreynosin (**9**)	3.607
Butyrylreynosin (**10**)	3.187
Octanoylreynosin (**11**)	5.303
Cynaropicrin (**12**)	0.046
Bis(4-fluorobenzoyl)cynaropicrin (**13**)	5.827
APO (**14**)	1.136
4-Fluorobenzoyl-*N*-APO (**15**)	2.970
DiS-OH (**16**)	3.019
Disulfanediylbis(2,1-phenylene) bis(4-fluorobenzoate) (**17**)	7.223
DiS-NH_2 (**18**)	2.736
N,N'-(Disulfanediylbis(2,1-phenylene))bis(4-fluorobenzamide) (**19**)	5.062
Gummiferolic acid (**20**)	7.180
4-Fluorobenzoic gummiferolic anhydride (**21**)	9.304

The results show that the sesquiterpene lactone derivatives tested (**4** and **5**) were more active than the benzoxazinoid mimic and etoposide against HeLa cells. IC_{50} values of 2.85 (**5**, R^2 = 0.9682), 14.53 (**4**, R^2 = 0.9783), 69.04 (**17**, R^2 = 0.9356) and 59.26 (etoposide, R^2 = 0.9765) were obtained, respectively, for HeLa cells. Furthermore, it is worth noting that compound **5** showed certain specificity between the two cell lines tested. Cell viability values of less than 50% were noted at 1 and 5 µM against tumoral cells, while values of 89% were obtained for the same concentrations against non-tumoral cells. In order to corroborate these findings, the selectivity index (SI) was calculated. This index

(expressed as IC_{50} ratio in HEK-293 versus HeLa cells) allows a determination of the selectivity of a compound on the cell lines tested, with a high selectivity corresponding to an SI value above 3.[24] A high selectivity value (SI = 5.63) was obtained for compound **5** whereas lower selectivities were determined for derivatives **4** and **17** (SI ≤ 3). This new derivative could be a promising lead compound since it is synthesized in only two steps from costunolide (multigram-scale production), which in turn is readily available (100 mg of costunolide/1 g of extract). In contrast, etoposide is produced semi-synthetically from (−)-podophyllotoxin extracted from *Sinopodophyllum hexandrum* T.S.Ying (Himalayan mayapple) on a milligram scale. Furthermore, new etoposide production strategies are being developed due to etoposide shortages in the past decade and as the species from which it is obtained is considered to be endangered.[25]

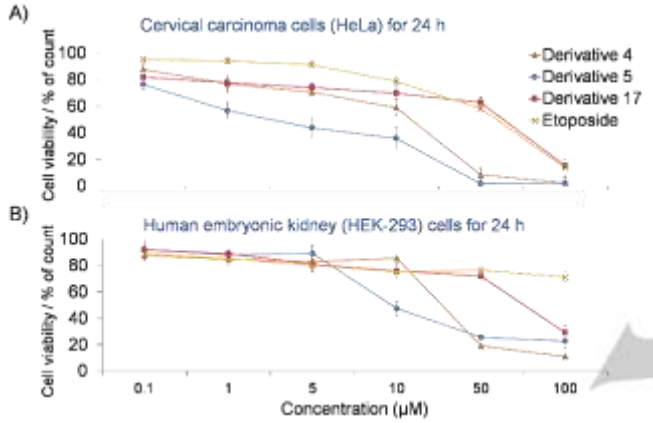

Figure 5. Cell viability by dye exclusion of derivatives **4**, **5**, **17** and the positive control (etoposide) at various concentrations against: A) cervical carcinoma (HeLa) and B) human embryonic kidney (HEK-293) cells, both for 24 h. Experiments were performed in triplicate and data are expressed as mean ± SD.

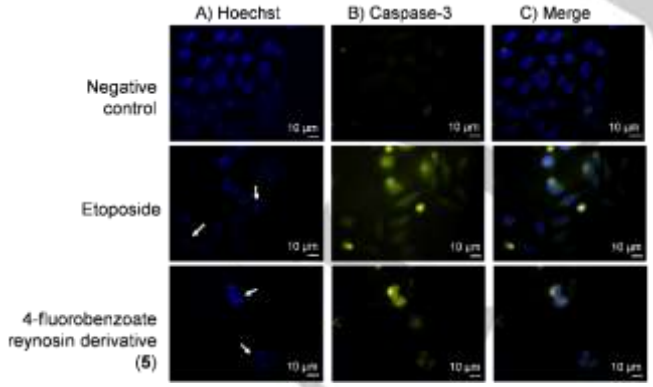

Figure 6. (A) DNA fluorescence staining by Hoechst (B) immunofluorescence staining results of Caspase-3 and (C) merged in Lane 3, after treatment with negative control (DMSO 0.1%), positive control (etoposide) and 4-fluorobenzoate reynosin derivative (**5**) at 100 µM for 20 h on HeLa cells.

In the case of compound **5**, programed suicide death by apoptosis was assessed. Apoptosis can be intrinsically activated by the release of cytochrome C from mitochondria or extrinsically activated by death receptors. Both pathways lead to the activation of a series of caspases that mediate the cell destruction. Caspase-3 is considered to be the most important of the executioner caspases and it is activated by any of the initiator caspases. Activation results in DNA fragmentation and PARP (Poly (ADP-Ribose) Polymerase) cleavage, which in turn triggers a caspase-dependent apoptotic signaling cascade.[26,27] In this study, immunofluorescence analysis was used to detect caspase-3. The results reveal that the expression intensity was higher after treatment with compound **5** in comparison to the negative control (0.1% DMSO) (Figure 6). DNA fragmentation could also be observed (indicated with arrows).

Molecular dynamics simulation

In order to delve further into the lipophilicity and bioactivity results, a molecular dynamics simulation was carried out on the cellular membrane. A total of 128 molecules of dipalmitoylphosphatidylcholine (DPPC) were employed to generate the bilayer. The cubic box simulation space was then solvated and Na^+ and Cl^- ionic species were added to simulate the ionic strength of a real cell.

Three markedly different lipophilic derivatives were used in this study to elucidate more varied behavior: reynosin (**2**), octanoylreynosin (**11**) and 4-fluorobenzoylreynosin (**5**). Specifically, 4-fluororeynosin was the most active compound, so this study allowed us to pinpoint the behavior that could explain the bioactivity results. These compounds were placed in the center-of-mass of the box, in the middle of bilayer, parallel to DPPC molecules, and the performance was analyzed during 10 ns to ascertain whether the compounds could move easily through the phospholipid, or if they are stabilized in one phase of the micellar simulation.

It can be seen in Figure S1 how reynosin (**2**) is displaced from the mass-center to the interface between the DPPC molecules and water above and below the bilayer. This finding is consistent with the behavior expected for its lipophilicity value (CLogP = 1.183). Nevertheless, this compound could be retained when the phosphatidyl and choline groups of the DPPC were solvated by water, as shown in Table 2. Reynosin (**2**) presents the strongest interaction with DPPC and also with water molecules, both of which support its amphiphilic behavior as expressed in Figure S1E, where at the end of the simulation reynosin (**2**) has the same spatial layout as DPPC. After 10 ns of simulation it can be observed how the lactone ring of the molecule becomes oriented towards the aqueous phase, with the dipole moment pointing towards the water. This situation is in agreement with that represented in Figure 8.

The RMSD plot (Figure 7A) of this compound shows significant fluctuations due to the dipole orientation, but it is stable at around 1.5 Å during the 10 ns simulation. These low variations are indicative of the high stability of reynosin (**2**) in the position represented in Figure 7A. This means that this compound will encounter problems in the membrane–crossing processes and it will be retained at the interface.

In the case of octanoylreynosin (**11**) the dipole moment changes markedly with respect to reynosin. Instead of being oriented towards the eudemasne skeleton, the carbonyl group provides

sufficient polarity to move the dipole moment towards the six-membered ring in the sesquiterpene. Notwithstanding, it can be seen from Figure 7C and Figure S2 that the molecule changes its conformation to orient the long saturated chain parallel to the DPPC molecules and the eudesmane fragment is in the same spatial layout as reynosin (**2**).

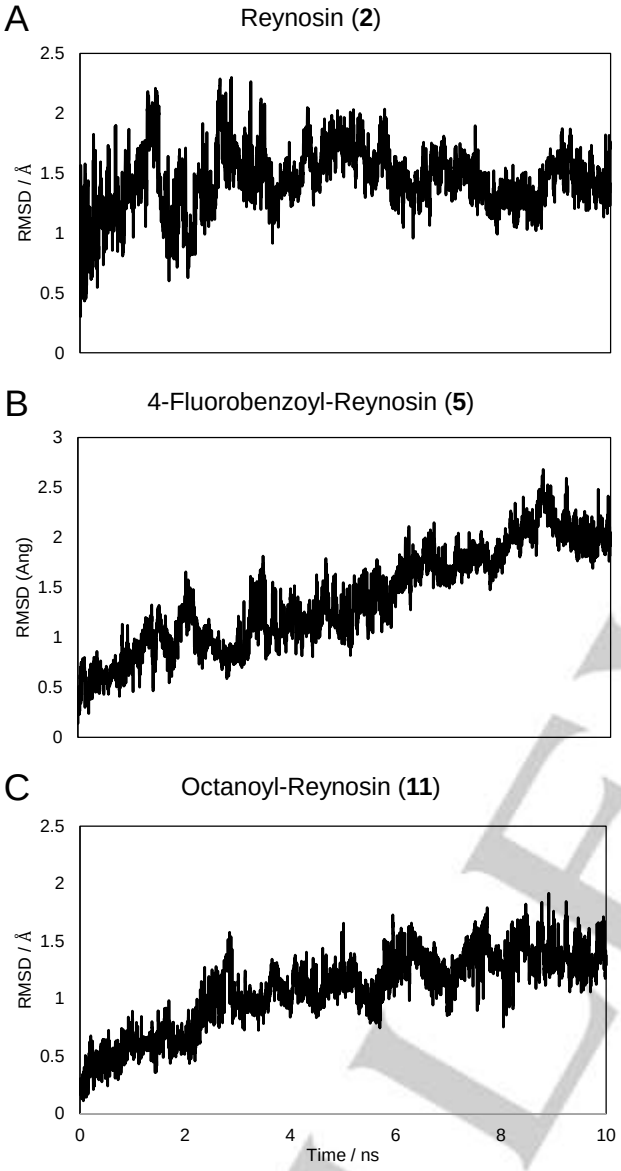

Figure 7. RMSD plot of reynosin (**2**) (A), 4-fluorobenzoyl-reynosin (**5**) (B) and octanoyl-reynosin (**11**) (C) in the simulated membrane system.

The octanoyl ester derivative **11** has a high lipophilicity value (CLogP = 5.303), which is more similar to that of DPPC (CLogP = 4.004) than reynosin (**2**). However, according to the data in Table 1 compound **11** has a lower binding energy. This fact can be explained by the lower energetic interaction between the non-polar groups than interactions such as hydrogen bonds established by polar groups.

The RMSD plot in Figure 7C showed a small but continuous fluctuation from the start to the end of the MD simulation. Nevertheless, the RMSD did not exceed 1.5 Å. In addition, the snapshots observed in Figure S2 do not show any significant movements of the molecules and they remain in the middle of the bilayer in all cases. The diffusion coefficient of octanoylreynosin (**11**) is the lowest of all of the tested compounds and this is due to the high molecular volume according to the Stokes–Einstein equation (Equation 1), with a similar value to the DPPC molecule, which hinders the movement by diffusion. All of the results outlined above, i.e., RMSD plot, energy values and diffusion coefficient, lead us to believe that this compound will not easily pass through the membrane and, as a consequence, it has a lower bioactivity than the other two compounds simulated.

$$D = \frac{k_B \cdot T}{6 \cdot \pi \cdot \eta \cdot r}$$

Equation 1. Stokes–Einstein relation for the diffusion coefficient, where the constant r is related to the radius of the molecule, which in turn is directly proportional to molecular volume. (k_B is the Boltzmann constant, T is the temperature and η is the dynamic viscosity).

Table 2. Summary of molecular dynamics simulations data acquired for each derivative at 298 K.

System/Values	Reynosin (**2**)	Octanoyl-Reynosin (**11**)	Fluoro-Reynosin (**5**)
DPPC-Lig Energy (Kcal/mol)	–26.4976	–9.5189	–2.88359
Water-Lig Energy (Kcal/mol)	–9.33472	–6.7482	–3.04115
DPPC Diffusion Coef. (cm^2/s) (10^{-5})	0.0163 ± 0.0051	0.0084 ± 0.0033	0.0074 ± 0.0016
Lig Diffusion Coef. (cm^2/s) (10^{-5})	0.0312 ± 0.0675	0.0269 ± 0.0051	0.1115 ± 0.0640

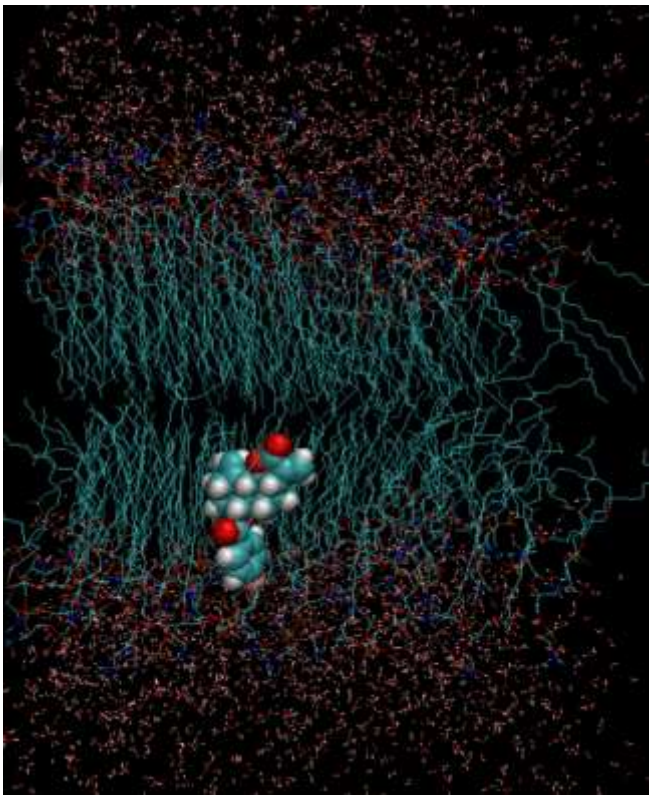

Figure 9. Snapshot of 4-fluorobenzoyl-reynosin (**5**) after 10 ns of molecular dynamics in the simulated membrane system.

4-Fluorobenzoylreynosin (**5**) shows the highest interaction energy with DPPC and water molecules. In addition, compound **5** has the highest diffusion coefficient, which could indicate an easy passage through the membrane. The diffusion coefficient is quite remarkable as it is three- and four-fold higher than the values for reynosin (**2**) and octanoylreynosin (**11**), respectively. Furthermore, the calculated diffusion coefficient is comparable to that of pyridine in water ($2.8 \cdot 10^{-6}$ cm^2/s).[28]

This derivative has the best lipophilicity value to be considered as a good drug candidate, according to Lipinski's rule (CLogP = 4.201), as a compromise between water solubility and interaction with fatty derivatives (DPPC). Furthermore, fluctuations along the simulation are the most relevant in comparison with others, as shown by the RMSD plot in Figure 7B. Changes from 0 to 2.5 Å in a steady rise are also observed in the snapshots (Figure 9), which means that the compound is not retained to any extent and it can move more easily than other derivatives from the aqueous phase through the DPPC molecules.

It can be observed from Figure S3 that the fluoro-substituted fragment, which is the most polar unit, is oriented towards the water phase and the dipole moment points towards the phosphatidyl and choline groups.

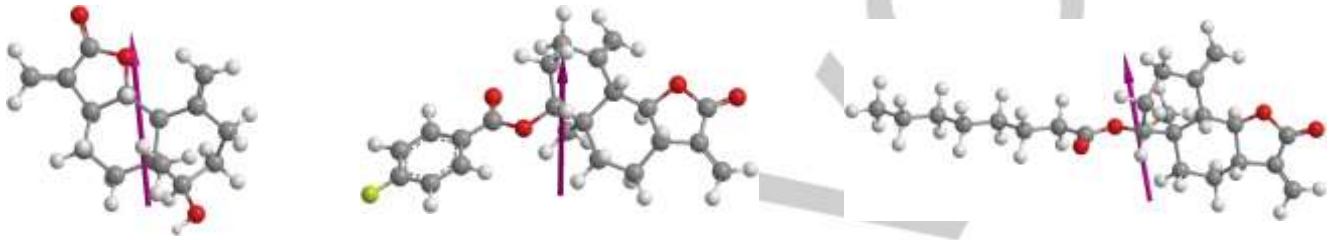

Reynosin
Dipole moment: 6.2652 Debye

Fluor-Reynosin
Dipole moment: 6.3349 Debye

Octanoyl-Reynosin
Dipole moment: 6.2082 Debye

Figure 8. Calculated dipole moments for three derivatives selected for MD simulations employing HF/6-31G.

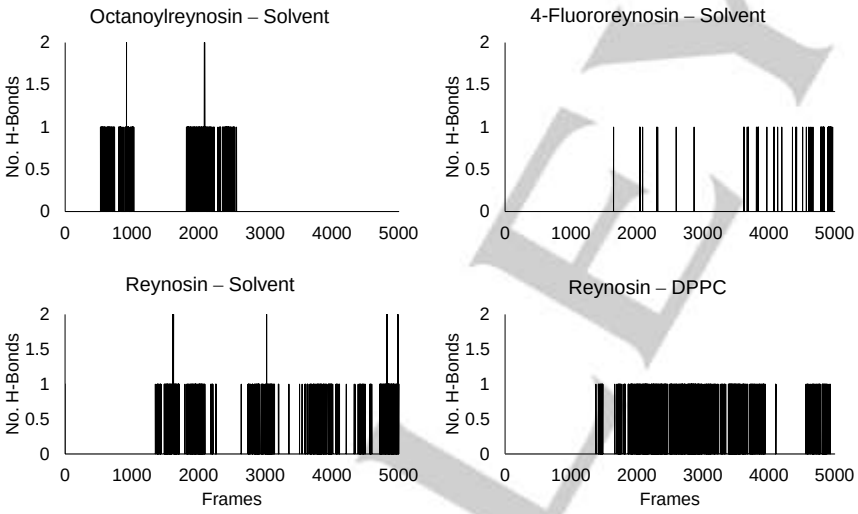

Figure 10. Analysis of hydrogen bonds for each bioactive molecule with the solvent and DPPC at every step of the molecular dynamics simulation. All molecules interact with the solvent, but only reynosin (2) forms H-bonds with DPPC.

A hydrogen bond analysis fixed at a distance of 3.0 Å and 20 degrees as the cut-off angle showed that reynosin (**2**) is the only compound that is able to establish this intermolecular interaction with DPPC molecules due to its hydroxyl group. Only two hydrogen bonds were established, with DPPC79 and DPPC75 (12.84% and 1.49% of occupancy, respectively), but these had a long lifetime (Figure 10) and high occupancy throughout the 10 ns of the simulation. The interaction of reynosin (**2**) with the solvent was also the most abundant but this had a shorter lifetime than the H-bonds with DPPC. The occupancies of the atoms involved did not exceed 2.5% (Table S14) – in contrast with data for occupancy with the DPPC. This finding supports the RMSD plot and snapshots shown in Figure 7A, which indicates a very stable arrangement of the compound in the membrane and high energetic interaction with the polar fragment of the DPPC in the interphase.

Neither octanoylreynosin (**11**) nor 4-fluorobenzoylreynosin (**5**) form hydrogen bonds with DPPC molecules and these compounds show a similar number of hydrogen bonds with the solvent (Table S15 and S16). Nevertheless, octanoylreynosin (**11**) only forms H-bonds in the early steps of the molecular dynamics simulation (before 4 ns). The structural similarity with DPPC molecules means that **11** is located in the middle of the membrane and it establishes other secondary interactions with phosphatidyl derivatives (DPPC). In the case of 4-fluorobenzoylreynosin (**5**), the solvent donor hydrogen bond interaction has the lowest occupancy, with values below 0.4%. However, these bonds are present in all stages of the MD. This means that the molecule switches throughout the simulation and bonds with different solvent molecules, as shown in Figure 7B, and this facilitates membrane crossing.

Conclusion

Natural hydroxylated derivatives of costunolide remain relevant for future drug development. These compounds have previously had important applications against different tumors, but ester derivatives have never been tested. Eight ester-eudesmane derivatives have been synthesized in quantitative yield in a one-

pot synthesis from a starting material that can be obtained on multi-gram scale from plant material.

Ester-eudesmane derivatives showed strong cytotoxicity against HeLa cells, with values of less than 20% cell viability observed in most cases after 24 hours of treatment. The derivatives with an aromatic framework were more active than compounds with a linear ester chain. In view of these findings, other mimics and natural compounds were modified by introducing a 4-fluorobenzoyl core. However, the boost in bioactivity shown by reynosin esters does not have a counterpart in other natural products. Overall, the modification of amino groups to yield amide derivatives led to a decrease in the activity, while the best results were obtained by modifying the hydroxyl groups to form ester derivatives. It is worth highlighting the potential cytotoxic effects of compounds **4**, **5** and **17**. These findings encouraged us to perform a cell viability study with these promising compounds at various concentrations against tumoral (HeLa) and non-tumoral (HEK-293) cells. It is worth noting the high selectivity of derivative 5 between the two cell lines tested, with a selectivity index above three. Immunofluorescence staining analysis showed that this derivative induces apoptosis and DNA fragmentation on HeLa cells.

In an effort to elucidate the origin of the bioactivity, molecular dynamics simulations were carried out with a cell membrane construction and the cross-membrane processes was linked with the cell viability results. These simulations showed how 4-fluorobenzoylreynosin (**5**) is not retained by either phosphatidyl derivatives (DPPC) that constitute the membrane or solvent molecules, so it can move through the system more easily than reynosin (**2**) or other derivatives. This compound has the highest diffusion coefficient and establishes hydrogen bonds with a short lifetime, which could explain theoretically the level of bioactivity.

Experimental Section

Chemicals. For the cytotoxicity bioassays, Dulbecco's Modified Eagle's Medium (DMEM) was supplied by Lonza (Verviers, Belgium), premixed phosphate buffer saline solution (PBS, 10X) was supplied by Roche (Steinheim, Germany), fetal bovine serum, penicillin/streptomycin, l-glutamine, sodium pyruvate, trypsin and minimum essential medium non-essential amino acids (MEM NEAA) were purchased from Gibco (Paisley, UK). Anti-active caspase 3 rabbit polyclonal antibody, fluorescein isothiocyanate (FITC)-conjugated goat anti-rabbit IgG, etoposide and trypan blue solution (0.4%) were purchased from Sigma Aldrich (Steinheim, Germany). Bisbenzimidine H 33342 fluorochrome (Hoechst) was obtained from Calbiochem. 4-Fluorobenzoyl chloride, benzoyl chloride, 3-fluorobenzoyl chloride, 4-chlorobenzoyl chloride, fluorobenzoic acid, butyryl chloride, octanoyl chloride, 2-aminothiophenol, 2-hydroxythiophenol, *meta*-chloroperbenzoic acid were supplied by Sigma-Aldrich®. 2,4,6-Trifluorobenzoyl chloride and *p*-TsOH were supplied by Alfa-Aesar®.

Cell lines and cell cultures. HeLa (human cervix carcinoma) and HEK-293 (human embryonic kidney 293) cells were cultured as monolayers in DMEM (GIBCO) supplemented with 10% fetal bovine serum, 5% glutamine, 5% non-essential amino acids, 5% penicillin-streptomycin and 5% sodium pyruvate. Cells were maintained in a HERA Cell 150i (Thermo Scientific) incubator at 37 ºC, 5% CO_2 and 95% humidity.

Cell viability assays. Tumoral (HeLa) and non-tumoral cells (HEK-293) were used for the experiments. 1.5 × 105 cells per mL were seeded in 6-well plates (VWR, Germany) in complete medium. Compounds were dissolved in DMSO (0.1% v/v) at the appropriate concentration for 24 h. Control cultures, including cells treated either with 0.1% DMSO or etoposide, were also included in each experiment. Cell viability was evaluated by the Trypan blue dye exclusion assay. Trypan blue solution was mixed 1:1 with a sample of control or treated cells. After incubation for 2 min, a fraction of blue-stained cells was assessed using an Automated TC20 Cell Counter (Bio-Rad). IC_{50} values were determined with GraphPad (Prism software v. 5.00). All experiments were repeated at least three times with similar results. The results are expressed as the mean ± S.D.

Immunofluorescence staining. HeLa cells were grown on 11 mm × 22 mm coverslips (Thomas Scientific, USA) until 70% of confluence and then incubated for 20 h with 4-fluorobenzoate reynosin derivative (**4**) or etoposide (positive control) at 100 µM in culture medium as described above. Caspase-3 activity assay was performed according to the manufacturer's protocol.[29] In brief, cover slips with HeLa cells were fixed in methanol for 10 min at –20 ºC, later washed in PBS, and incubated with the primary rabbit active caspase-3 antibody at 1:500 dilution in PBS for 45 min at 37 ºC. Thereafter, cells were washed in PBS in triplicate for 5 min each and incubated with the secondary antibody fluorescein isothiocyanate (FITC)-conjugated goat anti-rabbit IgG (dilution 1:100) in PBS for 45 min at 37 ºC. Finally, cells were washed three times with PBS, and mounted in PBS–glycerol containing Hoechst at 1 µg/ml. The expression of Caspase-3 in cells was observed under a Zeiss Axiophot fluorescence microscope (Carl Zeiss, West Germany) equipped with a Zeiss Axiocam 503 camera.

Isolation of costunolide (1). *Saussurea costus* CH_2Cl_2 root extract (50.0 g) was employed for the isolation of 2.5 g of costunolide. 6 L of hexane/ethyl acetate 5% was used to purify the compound by column chromatography.

Synthesis of reynosin (2) and santamarine (3). The method of Zorrilla *et al.* with modifications was employed.[30] Costunolide (100 mg, $4.30 \cdot 10^{-4}$ moles) was dissolved in CH_2Cl_2 (6 mL). *m*-CPBA (89 mg, $5.16 \cdot 10^{-4}$ moles, 1.2 eq.) was added to the above solution and the reaction mixture was stirred at room temperature for 24 h. A catalytic amount of *p*-TsOH was added and the reaction mixture was stirred for a further 2 h. The mixture was extracted three times with 1.0 M NaOH and the combined organic phase was dried with anhydrous Na_2SO_4. Purification by CC was carried out with a Hexane:AcOEt gradient (80:20–50:50) to give santamarine (**2**) **(**58.8 mg, 58.8%) and reynosin (**3**) (30.5 mg, 30.5%).

Synthesis of 4-fluorobenzoylsantamarine (4). Santamarine (**2**) (30 mg, $1.21 \cdot 10^{-4}$ moles) was dissolved in dry pyridine (2 mL) under an inert atmosphere. Two equivalents of 4-fluorobenzoyl chloride ($2.42 \cdot 10^{-4}$ moles, 28.6 µL) were added to the flask and the reaction mixture was stirred for 12 h at room temperature. The mixture was extracted three times with saturated aqueous $CuSO_4$ and the organic phase was washed three times with 0.1 M NaOH solution. Chromatographic separation was carried out with a gradient from 10% to 40% (Hexane:AcOEt) to give the product in 85% yield. NMR data see Table S1, Figure S4 and S5. Calculated *m/z* for $[C_{22}H_{23}FO_4]Na^+$ 393.1473, obtained 393.1498. IR (cm^{-1}): 2935.5, 2854.3, 1771.0, 1716.9, 1603.1, 1507.8, 1271.2, 1237.4, 1114.9, 1090.3, 982.8, 964.6, 854.4, 767.3. UV (CH_3CN), λ_{max}: 244 nm.

General synthesis of acyl derivatives of reynosin (5–11). Reynosin (**3**) (30 mg, $1.21 \cdot 10^{-4}$ moles) was dissolved in dry pyridine (2 mL) under an inert atmosphere. Two equivalents of the acyl chloride (Table 2) were added to the flask and the reaction mixture was stirred for 12 h at room temperature. The mixture was extracted three times with saturated aqueous $CuSO_4$ and the organic phase was washed three times with 0.1 M NaOH solution. Chromatographic separation was carried out with a gradient from 10% to 40% (Hexane:AcOEt) to give the desired compounds in the yields shown in Table 3.

Table 3. Experimental data in synthesis of acyl derivatives

Compound	Volume (μL)	Yield (%)
4-fluorobenzoyl chloride (**5**)	28.6	88
benzoyl chloride (**6**)	28.1	99
4-chlorobenzoyl chloride (**7**)	31.0	85
3-fluorobenzoyl chloride (**8**)	29.0	86
2,4,6-trifluorobenzoyl chloride (**9**)	31.4	76
butyryl chloride (**10**)	25.1	87
octanoyl chloride (**11**)	41.3	80

4-Fluorobenzoylreynosin (**5**). NMR data see Table S2, Figure S6 and S7. Calculated *m*/*z* for $[C_{22}H_{23}FO_4]Na^+$ 393.1473, obtained 393.1492. IR (cm^{-1}): 2933.0, 2851.6, 1771.9, 1716.8, 1682.6, 1605.0, 1508.4, 1271.8, 1240.9, 1153.1, 1114.0, 1091.3, 854.7, 768.8. UV (CH_3CN), λ_{max}: 248 nm.

Benzoylreynosin (**6**). NMR data see Table S3, Figure S8 and S9. Calculated *m*/*z* for $[C_{22}H_{24}O_4]Na^+$ 375.1567, obtained 375.1576. IR (cm^{-1}): 2938.9, 2856.1, 1771.7, 1715.3, 1451.4, 1272.3, 1112.6, 965.8, 712.8. UV (CH_3CN), λ_{max}: 224 and 196 nm.

4-Chlorobenzoylreynosin (**7**). NMR data see Table S4, Figure S10 and S11. Calculated *m*/*z* for $[C_{22}H_{23}ClO_4]Na^+$ 409.1177, obtained 409.1180. IR (cm^{-1}): 2933.2, 2854.6, 1771.7, 1717.2, 1594.3, 1271.2, 1116.5, 1103.9, 1032.8, 760.0. UV (CH_3CN), λ_{max}: 239 and 197 nm.

3-Fluorobenzoylreynosin (**8**). NMR data see Table S5, Figure S12 and S13. Calculated *m*/*z* for $[C_{22}H_{23}FO_4]Na^+$ 393.1473, obtained 393.1483. IR (cm^{-1}): 2928.4, 2854.6, 1773.3, 1719.0, 1592.3, 1446.1, 1290,1. 1270.5, 1203.8, 1093.2, 966.1, 755.6. UV (CH_3CN), λ_{max}: 278, 225 and 192 nm.

2,4,6-Trifluorobenzoylreynosin (**9**). NMR data see Table S6, Figure S14 and S15. Calculated *m*/*z* for $[C_{22}H_{21}F_3O_4]Na^+$ 429.1284, obtained 429.1299. IR (cm^{-1}): 2938.8, 2850.0, 1772.5, 1730.0, 1641.8, 1618.4, 1444.9, 1272.4, 1130.0, 1048.3, 852.4. UV (CH_3CN), λ_{max}: 221 and 192 nm.

Butyrylreynosin (**10**). NMR data see Table S7, Figure S16 and S17. Calculated *m*/*z* for $[C_{19}H_{26}O_4]Na^+$ 341.1723, obtained 341.1731. IR (cm^{-1}): 2936.5, 2874.8, 1771.5, 1732.7, 1458.1, 1368.7, 1257.0, 1227.8, 1179.7, 1149.2, 1092.6, 1050.6, 986.5, 966.0. UV (CH_3CN), λ_{max}: 194 nm.

Octanoylreynosin (**11**). NMR data see Table S8, Figure S18 and S19. Calculated *m*/*z* for $[C_{23}H_{34}O_4]Na^+$ 397.2349, obtained 397.2330. IR (cm^{-1}): 2930.1, 2856.7, 1774.0, 1733.8, 1457.8, 1412.8, 1377.7, 1257.8, 1148.5, 1051.3, 966.2. UV (CH_3CN), λ_{max}: 196 nm.

Isolation of cynaropicrin (12). *Cynara cardunculus* var. *scolymus* AcOEt leaf extract (94.1 g) was employed to isolate 0.24 g of cynaropicrin. The isolation procedure was similar to that described in the literature.[31]

Synthesis of bis(4-fluorobenzoyl)cynaropicrin (13). Cynaropicrin (**12**) (30 mg, $8.66 \cdot 10^{-5}$ moles) was dissolved in dry pyridine (2 mL) under an inert atmosphere. Three equivalents of 4-fluorobenzoyl chloride ($2.60 \cdot 10^{-4}$ moles, 30.7 μL) were added to the flask and the reaction mixture was stirred for 12 h at room temperature. The mixture was extracted three times with saturated aqueous $CuSO_4$ and the organic phase was washed three times with 0.1 M NaOH solution. Chromatographic separation was carried out with a gradient from 0% to 30% (Hexane:Acetone) and HPLC was subsequently employed to obtain the product at 7.4 min (35% Hexane:Acetone) (45% yield) using a Merck-Hitachi system (Tokyo, Japan) with a refractive index detector (Elite LaChrom L-2490). A semipreparative LiChrospher 10 μm 250-10 Si 60 (Merck) column was employed with a flow rate of 3 mL/min. NMR data see Table S9, Figure S20 and S21. Calculated *m*/*z* for $[C_{33}H_{28}F_2O_8]Na^+$ 613.1644, obtained 613.1644. IR (cm^{-1}): 2927.7, 1770.2, 1722.3, 1603.2, 1508.2, 1270.3, 1241.1, 1153.6, 1113.7, 854.7, 768.1. UV (CH_3CN), λ_{max} 201 nm.

Synthesis of 2-amino-3*H*-phenoxazin-3-one (APO) (14). 2-Aminophenol (1 g, $9.16 \cdot 10^{-3}$ moles) was dispersed in a mixture 50:50 H_2O/MeOH and stirred during 24 hours while an oxygen flow was passed through at room temperature. A dark precipitate was obtained and this was filtered off. This solid was washed with cold water and recrystallized in $CHCl_3$ to give APO (99% yield).

Synthesis of 4-fluorobenzoyl-*N*-APO (15). APO (**14**) (30 mg, $1.59 \cdot 10^{-4}$ moles) was dissolved in dry pyridine (2 mL) under an inert atmosphere. 1.5 equivalents of 4-fluorobenzoyl chloride ($2.39 \cdot 10^{-4}$ moles, 28.2 μL) were added to the flask and the reaction mixture was stirred for 12 h at room temperature. The mixture was extracted three times with saturated aqueous $CuSO_4$ and the organic phase was washed three times with 0.1 M NaOH solution. Chromatographic separation was carried out with a gradient from 0% to 20% (Hexane:AcOEt) to give the target compound in 69% yield. NMR data see Table S10, Figure S22 and S23. Calculated *m*/*z* for $[C_{19}H_{11}F_2N_2O_3]H^+$ 335.0826, obtained 335.0846. IR (cm^{-1}): 3355.2, 2921.9, 2851.6, 1739.0, 1692.4, 1618.1, 1529.8, 1502.1, 1350.0, 1240.3, 1174.9, 880.7, 847.9, 755.1. UV (CH_3CN), λ_{max}: 255 and 410 nm.

Synthesis of 2,2'-disulfanediyldiphenol (DiS-OH) (16). This compound was synthesized by the method of Oliveira *et al.* with modifications.[32] 2-Hydroxythiophenol (100 mg, 0.82 μL, $7.93 \cdot 10^{-4}$ moles) was dissolved in acetone (35 mL). A solution of KIO_3 (1.36 g, 8 eq. $6.59 \cdot 10^{-3}$ moles) in water (100 mL) was added and

the mixture was stirred for 24 hours at room temperature. The mixture was extracted five times with AcOEt and the combined organic phases were dried (Na_2SO_4). No further purification was required to give DiS-OH (195 mg, 98% yield).

Synthesis of disulfanediylbis(2,1-phenylene) bis(4-fluorobenzoate) (17). DiS-OH (**16**) (100 mg, $4.00 \cdot 10^{-4}$ moles) was dissolved in dry pyridine (500 μL). Three equivalents of 4-fluorobenzoyl chloride ($1.20 \cdot 10^{-4}$ moles, 141.6 μL) were added and the reaction mixture was stirred for 24 h at room temperature. The mixture was directly separated by column chromatography with a gradient from 5% to 30% (Hexane:AcOEt) to give the target compound in 89% yield. NMR data see Table S11, Figure S24 and S25. Calculated *m/z* for $[C_{26}H_{16}F_2O_4S_2]Na^+$ 517.0350, obtained 517.0380. IR (cm^{-1}):1742.2, 1733.9, 1601.3, 1504.6, 1466.6, 1252.6, 1240.8, 1198.7, 1155.9, 1064.8, 1014.4, 856.7, 761.2, 749.8, 682.6, 625.6, 575.3. UV (CH_3CN), λ_{max}: 199 nm.

Synthesis of 2,2'-disulfanediyldianiline (DiS-NH_2) (18). This compound was synthesized by the method of Oliveira *et al.* with modifications.[32] 2-Aminothiophenol (1 g, 0.83 mL, $7.99 \cdot 10^{-3}$ moles) was dissolved in a 1:1 mixture of H_2O:ethanol (100 mL). The solution was stirred for 18 h with airflow until a solid precipitated. The solid was filtered off, washed with cold water and dried in a vacuum oven overnight to give the target compound in 80% yield.

Synthesis of *N,N'*-(disulfanediylbis(2,1-phenylene))bis(4-fluorobenzamide) (19). DiS-NH_2 (**18**) (100 mg, $4.03 \cdot 10^{-4}$ moles) was dissolved in dry pyridine (500 μL). Three equivalents of 4-fluorobenzoyl chloride ($1.21 \cdot 10^{-4}$ moles, 142.8 μL) were added and the reaction mixture was stirred for 24 h at room temperature. The mixture was separated by column chromatography employing a gradient from 5% to 30% (Hexane:AcOEt) to give the target compound in 81% yield. NMR data see Table S12, Figure S26 and S27. Calculated *m/z* for $[C_{26}H_{18}F_2N_2O_2S_2]H^+$ 493.0851, obtained 493.0865. IR (cm^{-1}): 3377.5 1770.4, 1676.5, 1601.7, 1576.7, 1525.2, 1500.5, 1431.2, 1311.4, 1295.2, 1233.8, 1162.6, 849.1, 757.0, 749.2, 575.6. UV (CH_3CN), λ_{max}: 264 and 319 nm.

Isolation of gummiferolic acid (20). *Margotia gummifera* CH_2Cl_2 root extract (592.5 g) was employed to isolate 17.58 g of gummiferolic acid. The extract was concentrated and crystallized from hexane/CH_2Cl_2 (1:1 mixture).

Synthesis of 4-fluorobenzoic gummiferolic anhydride (21). Gummiferolic acid (**20**) (100 mg, $2.50 \cdot 10^{-4}$ moles) was dissolved in dry pyridine (2 mL) under an inert atmosphere. Five equivalents of 4-fluorobenzoyl chloride ($1.25 \cdot 10^{-3}$ moles, 147.5 μL) were added and the reaction mixture was stirred for 72 h at room temperature. The mixture was extracted three times with saturated aqueous $CuSO_4$ and the organic phase was washed three times with 0.1 M NaOH solution. Chromatographic separation was carried out with a gradient from 0% to 40% (Hexane:AcOEt) to give the target compound in 22% yield. NMR data see Table S13, Figure S28 and S29. Calculated *m/z* for $[C_{32}H_{38}F_2O_5]^-$ 521.2682, obtained 521.2703. IR (cm^{-1}): 2932.1, 2871.2, 1797.0, 1730.9, 1713.7, 1602.6, 1507.8, 1455.6, 1381.8, 1235.3, 1156.8, 997.2, 847.7. UV (CH_3CN), λ_{max}: 203 nm.

Molecular dynamics simulations. Dipalmitoylphosphatidylcholine (DPPC) was chosen as the lipid molecule to simulate the biological membrane, with TIP3P as a model for water molecules. GROMACS (2019.6 version) was employed with the OPLS-AA force-field, which is optimal for liquids, solvated and pseudo-liquid simulations.[33] The ligand was generated with GaussView (6.0.16 version) and its topology and parameters were obtained by employing the SwissParam server (www.swissparam.ch).[34] 128 molecules of DPPC were added in a cubic box with at least 1 nm from the edges of the box and 2 nm distance between periodic simulated membrane images, to fulfill the minimum image convention. Sodium and chloride ionic species were added to simulate the physiological conditions while keeping the system neutral. The ligand employed in the simulation was placed on the center-of-mass of the bilayer, parallel to DPPC molecules. The system was minimized until the force was <1000.0 $kJ \cdot mol^{-1} \cdot nm^{-1}$ employing a short-range of electrostatic and van der Waals cut-off of 1.2 Å. The system was then equilibrated at constant volume-temperature (NVT) for 0.1 ns with an increment of 2 fs per step. Berendsend thermostat modification (V-rescale) was employed and the temperature was 298 K to avoid the phase transition of the DPPC (315 K). An isobaric-isothermal (NPT) equilibration was performed for 1 ns with increments of 2 fs per step, employing the Nosé–Hoover thermostat. The increment of time concerning the NVT was due to heterogeneity of the system because of slow lipid diffusion. The fully equilibrated system was submitted to molecular dynamics simulation for 10 ns with 2 fs per step. In this case, the Nosé–Hoover thermostat was used for temperature control and the canonical Parrinello–Rahman thermostat for pressure control. Finally, a correction of the trajectory was carried out by DPPC bilayer recentering within the cubic box.

Acknowledgements

This research was supported by the "Ministerio de Economía, Industria y Competitividad" (MINEICO), Spain, Project AGL2017-88-083-R. F.J.R.M. thanks the University of Cádiz for predoctoral support under grant 2018-009/PU/EPIF-FPI-CT/CP. The authors declare no competing financial interest.

Keywords: Eudesmanolide, Molecular Dynamics, Acyl Derivative, Natural Product, Caspase-3

[1] D. Camp, A. Garavelas, M. Campitelli, *J. Nat. Prod.* **2015**, *78*, 1370–1382.

[2] E. W. Coronado-Aceves, C. Velázquez, R. E. Robles-Zepeda, M. Jiménez-Estrada, J. Hernández-Martínez, J. C. Gálvez-Ruiz, A. Garibay-Escobar, *Pharm. Biol.* **2016**, *54*, 2623–2628.

[3] L. Liu, D. Liu, C. Xiang, W. Dai, B. Li, M. Zhang, *Nat. Prod. Res.* **2020**, *34*, 1563–1566.

[4] L. F. Ding, J. Su, Z. H. Pan, Z. J. Zhang, X. N. Li, L. D. Song, X. De Wu, Q. S. Zhao, *Phytochemistry* **2018**, *155*, 182–190.

[5] S. Lim, S. J. Lee, K. W. Nam, K. H. Kim, W. Mar, *Arch.*

Pharm. Res. **2013**, *36*, 485–494.

[6] A. Ham, D. Kim, K. Ho, S. Lee, K. Oh, J. Shin, W. Mar, *Brain Res.* **2013**, *1524*, 54–61.

[7] S. Choodej, K. Pudhom, T. Mitsunaga, *Planta Med.* **2018**, *84*, 329–335.

[8] R. Amici, C. Bigogno, R. Boggio, A. Colombo, S. M. Courtney, R. Dal Zuffo, G. Dondio, F. Fusar, S. Gagliardi, S. Minucci, et al., *ChemMedChem* **2014**, *9*, 1574–1585.

[9] K. R. A. Abdellatif, H. A. H. Elshemy, S. A. Salama, H. A. Omar, *J. Enzyme Inhib. Med. Chem.* **2015**, *30*, 484–491.

[10] K. S. Gavale, S. R. Chavan, N. Kumbhar, S. Kawade, P. Doshi, A. Khan, D. D. Dhavale, *Bioorganic Med. Chem.* **2017**, *25*, 5148–5159.

[11] J. Y. Cho, A. R. Kim, J. H. Jung, T. Chun, M. H. Rhee, E. S. Yoo, *Eur. J. Pharmacol.* **2004**, *492*, 85–94.

[12] W. H. Wu, T. Y. Chen, R. W. Lu, S. T. Chen, C. C. Chang, *Phytochemistry* **2012**, *83*, 110–115.

[13] S. K. Steffensen, H. A. Pedersen, K. B. Adhikari, B. B. Laursen, C. Jensen, S. Høyer, M. Borre, H. H. Pedersen, M. Borre, D. Edwards, et al., *J. Agric. Food Chem.* **2016**, *64*, 8235–8245.

[14] E. Flores-Giubi, N. Geribaldi-Doldán, M. Murillo-Carretero, C. Castro, R. Durán-Patrón, A. J. Macías-Sánchez, R. Hernández-Galán, *J. Nat. Prod.* **2019**, *82*, 2517–2528.

[15] S. Lim, S.-J. Lee, K.-W. Nam, K. H. Kim, W. Mar, *Arch. Pharm. Res.* **2013**, *36*, 485–494.

[16] N. Gören, H. Woerdenbag, C. Bozok-Johansson, *Planta Med.* **1996**, *62*, 419–422.

[17] S. K. Poole, C. F. Poole, *J. Chromatogr. B Anal. Technol. Biomed. Life Sci.* **2003**, *797*, 3–19.

[18] L. G. Danielsson, Y. H. Zhang, *TrAC - Trends Anal. Chem.* **1996**, *15*, 188–196.

[19] C.-M. Sun, W.-J. Syu, M.-J. Don, J.-J. Lu, G.-H. Lee, *J. Nat. Prod.* **2003**, *66*, 1175–1180.

[20] A. C. Beekman, H. J. Woerdenbag, W. Van Uden, N. Pras, A. W. T. Konings, H. V. Wikström, T. J. Schmidt, *J. Nat. Prod.* **1997**, *60*, 252–257.

[21] D. Siriwan, T. Naruse, H. Tamura, *Fitoterapia* **2011**, *82*, 1093–1101.

[22] C. A. Lipinski, F. Lombardo, B. W. Dominy, P. J. Feeney, *Adv. Drug Deliv. Rev.* **2001**, *46*, 3–26.

[23] K. Donthiboina, P. Anchi, P. V. Sri Ramya, S. Karri, G. Srinivasulu, C. Godugu, N. Shankaraiah, A. Kamal, *Bioorg. Chem.* **2019**, *86*, 210–223.

[24] P. Prayong, S. Barusrux, N. Weerapreeyakul, *Fitoterapia* **2008**, *79*, 598–601.

[25] B. J. Schultz, S. Y. Kim, W. Lau, E. S. Sattely, *J. Am. Chem. Soc.* **2019**, *141*, 19231–19235.

[26] H. Wang, J. Zhu, L. Jiang, B. Shan, P. Xiao, J. Ai, N. Li, F. Qi, S. Niu, *BMC Complement. Med. Ther.* **2020**, *20*, 180.

[27] S. Elmore, *Toxicol. Pathol.* **2007**, *35*, 495–516.

[28] C. L. Yaws, in *Transp. Prop. Chem. Hydrocarb.*, William Andrew Inc., **2009**, pp. 502–593.

[29] A. Yiallouris, I. Patrikios, E. O. Johnson, E. Sereti, K. Dimas, C. De Ford, N. U. Fedosova, W. F. Graier, K. Sokratous, K. Kyriakou, et al., *Cell Death Dis.* **2018**, *9*, 764.

[30] J. G. Zorrilla, C. Rial, R. M. Varela, J. M. G. Molinillo, F. A. Macías, *Phytochem. Lett.* **2019**, *31*, 229–236.

[31] C. Rial, P. Novaes, R. M. Varela, J. M. . Molinillo, F. A. Macias, *J. Agric. Food Chem.* **2014**, *62*, 6699–6706.

[32] S. C. C. Oliveira, C. K. Z. Andrade, R. M. Varela, J. M. G. Molinillo, F. A. Macías, *ACS Omega* **2019**, *4*, 2362–2368.

[33] R. Zangi, *ACS Omega* **2018**, *3*, 18089–18099.

[34] V. Zoete, M. A. Cuendet, A. Grosdidier, O. Michielin, *J. Comput. Chem.* **2011**, *32*, 2359–2368.

Entry for the Table of Contents

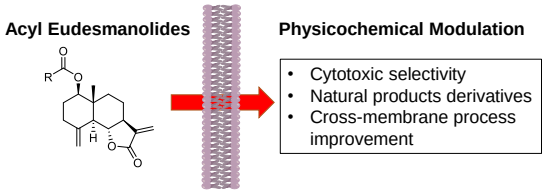

Acyl derivatives of different natural product families, have been synthesized and tested against tumoral and non-tumoral cell lines to identify selective derivatives with reduced negative impact upon application. The mode of action of these compounds was analyzed by anti-caspase-3 assays and molecular dynamics simulations provide evidence that lipophilicity plays a key role and the 4-fluorobenzoyl derivative can pass easily through the cell membrane.